2007

Metallated conjugated polymers as a new avenue towards high-efficiency polymer solar cells

WY Wong
Hong Kong Baptist University, rwywong@hkbu.edu.hk

XZ Wang

Z He

AB Djurisic

CT Yip

See next page for additional authors

This document is the authors' final version of the published article.
Link to published article: http://www.nature.com/nmat/journal/v6/n7/abs/nmat1909.html or doi:10.1038/nmat1909

Nature materials (accepted version)

ARTICLES

Metallated conjugated polymers as a new avenue towards high-efficiency polymer solar cells

WAI-YEUNG WONG[1,2*], XING-ZHU WANG[1], ZE HE[1], ALEKSANDRA B. DJURIŠIĆ[3#], CHO-TUNG YIP [3], KAI-YIN CHEUNG[3], HAI WANG[3], CHRIS S. K. MAK,[4] WAI-KIN CHAN[4]

[1] Department of Chemistry, Hong Kong Baptist University, Waterloo Road, Kowloon Tong, Hong Kong, P.R. China
[2] Centre for Advanced Luminescence Materials, Hong Kong Baptist University, Waterloo Road, Kowloon Tong, Hong Kong, P.R. China
[3] Department of Physics, The University of Hong Kong, Pokfulam Road, Hong Kong, P.R. China
[4] Department of Chemistry, The University of Hong Kong, Pokfulam Road, Hong Kong, P.R. China
E-mail: *rwywong@hkbu.edu.hk, # dalek@hkusua.hku.hk

Bulk heterojunction solar cells have been extensively studied due to their great potential for cost-effective photovoltaic devices. Although recent advances resulted in the fabrication of poly(3-hexylthiophene) (P3HT):fullerene derivative based solar cells with efficiencies in the range 4.4–5.0%, theoretical calculations predict that the development of novel donor materials with a lower band gap is required to exceed the power conversion efficiency of 10%. However, all the lower band gap polymers developed to date failed to reach the efficiency of P3HT based cells. To address this issue, we synthesized a soluble, intensely colored platinum metallopolyyne with a low band gap of 1.85 eV. The solar cells, containing metallopolyyne/fullerene derivative blends as the photoactive material, showed a power conversion efficiency with an average of 4.1%, without annealing or the use of spacer layers needed to achieve comparable efficiency with P3HT. This clearly demonstrates the potential of metallated conjugated polymers for efficient photovoltaic devices.

Bulk heterojunctions fabricated by blending polymers with fullerene have resulted in great improvements in the polymer photovoltaic cell efficiencies. The most commonly used materials for the fabrication of bulk heterojunctions are poly(3-hexyl)thiophene (P3HT) and [6,6]-phenyl C_{61}-butyric acid methyl ester (PCBM).[1–10] With optimized device structure and fabrication conditions, P3HT:PCBM bulk heterojunction solar cells can reach efficiencies as high as 4.4–5.0%.[1–3] However, novel materials with lower energy gaps need to be developed to improve the coverage of the solar spectrum and consequently improve the efficiency.[1] Therefore, great effort has been made to optimize the spectral response of polymer photovoltaic cells by extending the absorption to longer wavelengths, since absorption of the active layer must cover the major part of the solar spectrum. The lowering of the band gap of the polymer is predicted to result in efficiency exceeding 6%, while optimization of the energy levels and electron transfer to PCBM can lead to a further increase to ~ 8%.[11] The ultimate efficiency limit for fully optimized

polymer:fullerene solar cells is ~ 11%.[11] Other reports also predict that for power conversion efficiencies exceeding 10%, the donor polymer should have a band gap below 1.74 eV.[12] However, although several lower band gap polymers have been proposed for photovoltaic applications,[13–25] the highest reported power conversion efficiency was merely ~ 2.2%[17,18,20] to ~ 3.2%[21,22] which is lower than that of P3HT:PCBM cells. Obviously, there are a number of possible approaches to develop a polymer with electronic properties which have been identified as favourable by theoretical predictions. Yet limited success has been achieved with polymers based on polyfluorene,[12–16,18,23] benzothiadiazole,[24] or thiophene derivatives.[17,19,22,25]

One possible approach which has not been commonly explored involves the use of organometallic polymers. Although organometallic donor materials are commonly used in small-molecule solar cells,[26,27] soluble π-conjugated organometallic polyyne polymers have rarely been used in high-performance polymer solar cells.[28–30] The maximum photocurrent quantum efficiencies in single-layer neat platinum polyyne cells were ~ 0.04–1%,[28,31] while quantum efficiencies of ~ 1–2% could be achieved for these cells with the addition of 7 wt.-% of C_{60}.[29] More recently, an external quantum efficiency of ~ 9% has been achieved in bulk heterojunction cells using the metallopolyyne:PCBM composite, resulting in a power conversion efficiency of 0.27%.[30] The polymer absorbed only in the blue-violet spectral region with a maximum efficiency at 400 nm, and consequently the efficiency was low due to low coverage of the solar spectrum, although the photoinduced charge separation in the blend involved the triplet state of the organometallic polymer.[30] Obviously, the photovoltaic application of this type of materials is hampered by their wide band gaps, and possibly unfavourable energy levels and charge transport properties for forming efficient blends with PCBM. While polymetallaynes of the type *trans*-$[–Pt(PR_3)_2\text{-}C{\equiv}C\text{-}R\text{-}C{\equiv}C–]_n$ (R = carbocycles, heterocycles, main group elements, etc.) have

aroused much attention for use in optoelectronic devices,[28,31–33] most of these platinum(II) polyynes are usually characterized by relatively large band gaps,[34–37] which compare unfavourably with those of some conjugated organic polymers comprising alternating electron donor (D) and acceptor (A) units (< 1 eV).[38,39] However, successful strategies for creating narrow-band gap metallopolyynes involving the construction of D-A type systems are very scarce.[31,40] As a promising step towards our goal in designing metal polyynes of small band gaps, we have exploited 4,7-di-2'-thienyl-2,1,3-benzothiadiazole as a core component to create a new π-conjugated system with extended absorption that features unique D-A characteristics. The novel platinum metallopolyyne is based on planar conjugated segments with internal D-A functions between electron-rich Pt-ethynyl groups to achieve a low-band gap material (ca. 1.85 eV).

The synthesis of new platinum(II) polyyne polymer **P1** and its discrete model compound **M1** is shown in Scheme 1. They were prepared by the Sonogashira-type dehydrohalogenation reaction between $\mathbf{L_1}$ and the platinum chloride precursors.[37] **P1** was purified by silica column chromatography and repeated precipitation, leading to a dark purple powder of the polymer in good yield and high purity. Both metal compounds are thermally and air stable and soluble in common chlorinated hydrocarbons and toluene. **P1** can cast tough, free-standing thin films from its solution readily. Gel-permeation chromatography on **P1** suggests a high-molecular-weight material with the degree of polymerization ~ 22 (~ 66 heterocyclic rings in total). The structures were unequivocally characterized using elemental analyses, mass spectrometry, IR and NMR spectroscopies. The rigid-rod nature of **P1** was also confirmed by the X-ray crystal structure analysis on **M1** (Fig. 1).

The absorption and emission spectra of $\mathbf{L_1}$, **P1** and **M1** were measured in CH_2Cl_2 solutions at 298 K (Fig. 2). The absorption of a deep purple solution of **P1** is dominated by a strong band peaking at 554 nm, and the polymer exhibits an intense fluorescence band at 680 nm. The

absorption and emission properties of **M1** are very similar to that of **P1**, with the absorption maximum at 548 nm. The apparent lack of an energy shift in the electronic transition between **M1** and **P1** indicates that the lowest singlet excited state is confined to a single repeat unit in the polymer chain. The optical band gap, determined from the onset of absorption, is 1.85 eV for **P1**. Due to the presence of a more extended π-electron delocalized system throughout the chain and the creation of an alternate D-A chromophore based on a highly electron-accepting benzothiadiazole rings in combination with the electron-donating thiophene rings,[41–45] the band gap of **P1** is significantly lowered by ca. 0.35–0.70 eV relative to the purely electron-rich bithienyl (2.55 eV)[28] or electron-deficient benzothiadiazole (2.20 eV) linked counterpart,[46] both of which appear yellow in the solid and solution phases. This is a clear indication of the role of strong D-A interactions in **P1**, i.e., the bithienyl-benzothiadiazole hybrid here imparts gap-narrowing characteristics to **P1**. The idea behind the material design can be visualized in the way that a conjugated polymer is formed by a regular alternation of D- and A-like moieties, possibly separated by neutral parts. If the D and A regions are extended through the Pt centre and alkynyl units we have a case analogous to the inorganic n-i-p-i super lattice quantum well structures, resulting in a reduction of the band gap.[44] The measured lifetimes for **P1** and **M1** are very short and lie in the nanosecond range. Unlike other Pt polyynes, the low-temperature emission for **P1** has no vibronic structure and only a weak temperature dependence (Fig. 2c). Such observations and the small Stokes shift (< 0.40 eV) preclude the emitting state as a triplet but a singlet excited state instead. Again in contrast to Pt polyynes of higher band gaps,[28,46] we observed no emission from a triplet excited state over the measured spectral window between 1.2 eV and 3.1 eV. This is not surprising and is in accordance with the energy gap law for Pt-containing conjugated polymers, in which the nonradiative decay rate from the triplet state increases exponentially with decreasing triplet-singlet energy gap.[47] There is always a trade-off between the band gap and the rate of

phosphorescence in such system. In other words, a high-band-gap polymer with a high triplet state energy will normally favour the observation of triplet emission whereas the low-gap congener will probably not be phosphorescent even at low temperatures. A similar phenomenon has been observed for a low-band-gap Pt polyyne spaced by a thieno-pyrazine unit.[31,42] Therefore, it is not the triplet state but mostly a charge-transfer excited state that contributes to the efficient photoinduced charge separation in the energy conversion for **P1**,[31] which is different from the Pt-thiophene polyyne based blends where charge separation occurs via triplet state of the polymer.[30] From these results, we attribute the localized state centred at 2.22 eV to a strong D-A charge-transfer type interaction. The charge-transfer nature of the transition was also supported by the solvent dependent emission spectra of **P1** in solvents of different polarities. **P1** exhibited a marked positive solvatochromism with a red-shift of the emission maximum of ~ 40 nm from toluene (λ_{em} = 670 nm) to $CHCl_3$ (λ_{em} = 710 nm), which suggests a less polar excited state (see Supporting Information). We consider that the D-A interaction already present in the 4,7-di-2'-thienyl-2,1,3-benzothiadiazole unit is remarkably enhanced by the extensive π-delocalization in the polymer backbone containing the electron-rich platinum ion. This causes a charge-transfer type transition which leads to a substantial lowering of the optical gap. **P1** shows an irreversible oxidation wave at +0.57 and a reversible reduction peak at –1.66 V in CH_2Cl_2. The oxidation (E_{ox}) and reduction (E_{red}) potentials were used to determine the HOMO and LUMO energy levels using the equations $E_{HOMO} = -(E_{ox} + 4.8)$ eV and $E_{LUMO} = -(E_{red} + 4.8)$ eV which were calculated using the internal ferrocene standard value of –4.8 eV with respect to the vacuum level.[48] Hence, the calculated HOMO and LUMO energies are –5.37 and –3.14 eV, respectively.

Polymer solar cells were fabricated by using **P1** as an electron donor and PCBM as an electron acceptor. The hole collection electrode consisted of indium tin oxide (ITO) with a spin-coated poly(3,4-ethylene-dioxythiophene)-poly(styrene sulfonate) (PEDOT:PSS), while Al served

as the electron collecting electrode. Different solvents, solution concentrations, and spinning speeds were tested to identify optimal fabrication conditions for **P1**:PCBM blend cells. Toluene was identified as the solvent resulting in the best performance, followed by chlorobenzene, while cells prepared from chloroform and xylene solutions exhibited significantly worse performance. The optimal concentration and spinning speed resulted in the layer thickness of 70–75 nm, as verified by a step-profiler and spectroscopic ellipsometry (JA Woollam V-VASE), while the thickness of PEDOT:PSS was ~ 27 nm. Solar cells with P3HT:PCBM active layers were also prepared for comparison. Since the performance of P3HT:PCBM cells is known to be strongly dependent on the material properties and processing conditions,[4] same processing conditions (apart from solution preparation due to solubility differences) were chosen for P3HT:PCBM solar cell. Since P3HT:PCBM cells have been extensively studied, we have cited relevant literature for the best performance of P3HT:PCBM cells instead of optimizing fabrication conditions for this type of cells. Considerable increase in the short circuit current density and the power conversion efficiency can be observed in the case of **P1** (Fig. 3). The obtained open circuit voltage for the best cell was V_{oc} = 0.82 V, short circuit current density was J_{sc} = 15.43 mA cm^{-2}, and the fill factor was FF = 0.39, resulting in the power conversion efficiency η = 4.93%. The open circuit voltage is also higher compared to P3HT:PCBM cells, which is likely due to the lower HOMO level of **P1** (–5.37 eV, compared to –5.20 eV for P3HT[1]). The P3HT:PCBM cell exhibited V_{oc} = 0.74 V, J_{sc} = 6.22 mA cm^{-2}, FF = 0.35, and η = 1.61%. It should be noted that the efficiency of our P3HT:PCBM cells is lower compared to the best reported results in the literature.[1–3] However, such high efficiencies require either more complicated device structure including a spacer layer[1] or annealing[2–6] to improve the cell performance.

It should also be noted that we use a different blend ratio (1:4 w/w) compared to that commonly used in P3HT:PCBM cells, which are typically 1:1[3–7] or 1:0.8[1] since it has been shown that the optimal blend ratio was in the range of 1:0.9–1:1.[7] However, optimal blend concentration is dependent on the polymer used. For **P1**:PCBM blends, cells with 1:4 ratio resulted in the best performance, similar to the case of poly[2-methoxy-5-(3',7'-dimethyloctyloxy)-1,4-phenylene vinylene] (MDMO-PPV):PCBM blends,[49,50] as well as poly(3-octylthiophene-2,5-diyl-*co*-3-decyloxythiophene-2,5-diyl):PCBM blends.[19] The improved cell performance for 1:4 ratios in MDMO-PPV:PCBM blends was attributed to improved charge transport and improved dissociation efficiency.[50] Atomic force microscopy (AFM) was used to characterize the blends of **P1**:PCBM with ratios of 1:4 and 1:1, as shown in Fig. 4. It can be observed that, similar to (MDMO-PPV):PCBM blends, phase separation occurs for 1:4 blend ratio while films with 1:1 ratio are smooth (~ 3–5 nm for 1:1 vs. ~ 20 nm for 1:4 ratio) and do not show significant phase separation and formation of larger PCBM domains. Similar film roughening and formation of larger PCBM aggregates is also observed in annealed P3HT:PCBM 1:1 blends which result in high solar cell efficiency.[2] Phase separation with formation of PCBM rich domains facilitates improved charge transport and carrier collection efficiency, which results in the reduction of recombination losses and the increase in short circuit current density.[49,51] Consequently, the performance of **P1**:PCBM cells with 1:4 blend ratio is improved compared to 1:1 ratio.

To investigate reasons for the improved efficiency, the external quantum efficiency (EQE) for solar cells with both active materials has been measured, as shown in Fig. 5a. The cells with **P1**:PCBM active layer exhibit a higher maximum EQE (87% vs. 67% for P3HT:PCBM) and a wider coverage of the visible spectral range, as expected from the absorption spectrum of the active layer (see inset of Fig. 5a). Charge transport in **P1**:PCBM and P3HT:PCBM layers was studied using time-of-flight (TOF) technique and space charge limited current (SCLC) modelling.

Experimental results for the electric field dependences of the electron and hole mobilities are shown in Fig. 5b and c. For TOF measurements, drop-casting technique had to be used instead of spin-coating to achieve sufficiently thick films, which involved very slow drying of the film in a solvent saturated atmosphere. As a result, in addition to increased roughness of the films compared to spin-coated films, the slow drying inherent to drop-casting process would also affect the mobility of the films, since it has been shown that slow drying of P3HT:PCBM films results in a significant enhancement of the hole mobility, leading to a more balanced charge transport.[9,52] It can be observed that electron and hole transport is more balanced in **P1**:PCBM blends, while both blend films exhibit small negative electric field dependence, in agreement with previously reported results for P3HT:PCBM blends.[52] The TOF and SCLC data for **P1**:PCBM blends give comparable hole and electron mobilities, although mobilities obtained from TOF measurements are lower. However, TOF measurement yields comparable hole and electron mobility in P3HT:PCBM blends, while SCLC model gives higher electron compared to hole mobility, which would be expected from the blend film composition in agreement with previous results.[53] Thus, the mobilities obtained from SCLC measurements can be considered more representative for describing the performance of solar cells prepared by the same fabrication method (spin-coating). Therefore, **P1**:PCBM blends exhibit balanced charge transport, as required for efficient solar cell performance,[53] and the mobility values are comparable to those measured in P3HT:PCBM cells with optimal (1:1) blend ratio reported in the literature.[52,53] However, it should be noted that the fill factor of the devices is relatively low, which can be a sign of space charge limited photocurrent.[10,50] The photocurrent dependence on the light intensity for voltages approaching V_{oc} ($V_0 - V = 0.2$ V) shows the slope ~ 3/4, which indicates the possibility of space charge limited device performance. Device performance is also very sensitive to atmosphere (oxygen and moisture) exposure, which likely results in the presence of traps and worsening of fill factor.

Comprehensive study of charge transport and the influence of traps is necessary to further improve the fill factor and device performance.

To investigate in more detail the reasons for excellent performance of **P1**:PCBM cells, we performed spectroscopic ellipsometry measurements of **P1**:PCBM and P3HT:PCBM blend films. The obtained real and imaginary parts of the index of refraction are shown in Fig. 5 d and e. It can be clearly observed that the extinction coefficient of **P1**:PCBM blend is higher above 550 nm, leading to improved absorption of the solar radiation. Typically, in the design of low-band gap polymer solar cells, the main concerns are the HOMO and LUMO levels of the polymer,[11,12] and charge transport in the cells.[11] However, the amount of the absorbed light is dependent not only on the cut-off wavelength of the absorption, but also on how intense the absorption is. Therefore, the design of the low-band gap polymers for photovoltaic applications should consider not only lowering the gap but also increasing the absorption coefficient of the polymer.

The performance of the devices with optimal composition and active layer thickness was studied in detail. The *J*–*V* curves under different excitation powers and the power dependence of the solar cell parameters are shown in Fig. 6. The short circuit current density exhibits a linear dependence on the optical power, while V_{oc} and FF show some increase and then saturate at higher intensity, which is expected.[26] To test the reproducibility of the results obtained, a large number (90) of cells were prepared. The solar cell performance parameters were (average value ± standard deviation) $V_{oc} = 0.82 \pm 0.03$ V, $J_{sc} = 13.1 \pm 3.2$ mA cm^{-2}, FF = 0.37 ± 0.03, and $\eta = 4.1 \pm 0.9$ %. If we compare only the devices within the same batch (fabricated from the same solution, electrode evaporated at the same time, 6–8 cells), much smaller variations were obtained, with $V_{oc} = 0.80 \pm 0.02$ V, $J_{sc} = 15.1 \pm 2.2$ mA cm^{-2}, FF = 0.40 ± 0.04, and $\eta = 4.8 \pm 0.4$ %. Overall, the reproducibility of the results was very good, and it is expected that it would be further improved if the fabrication was performed in nitrogen instead of air atmosphere. Although spectral mismatch

correction has not been performed,[54] there is a good agreement between the measured short circuit current density and the short circuit current density estimated from EQE and theoretical AM1.5 global solar spectrum, with on average 1.4 mA/cm^2 difference between the measured J_{sc} and J_{sc} estimated from EQE, which is smaller than the standard deviation of the J_{sc} values of different cells. In addition, the measurements of the same devices in our laboratory and at CEA-INES, Laboratoire Composants Solaires, were in excellent agreement. We anticipate that the performance of these devices can be further improved by device optimization, as well as further chemical modifications of these metallized systems. It is expected that this demonstration will stimulate further work on the development of novel organometallic polymers for photovoltaic applications and bring bulk heterojunction polymer photovoltaic devices closer to commercialization.

METHODS

All chemicals for the syntheses were purchased from Aldrich or Acros Organics. PCBM and regioregular P3HT (M_w 20,000–50,000) were purchased from American Dyes. PEDOT:PSS (Baytron P VPAI 4083) was purchased from H. C. Starck. Reactions and manipulations were carried out under an atmosphere of prepurified nitrogen using Schlenk techniques. The cyclic voltammetry experiment of the polymer film was performed by casting the polymer on the glassy-carbon working electrode with a Pt wire as the reference electrode, at a scan rate of 100 mV s^{-1}. The solvent in all measurements was deoxygenated MeCN, and the supporting electrolyte was 0.1 M [^{n}Bu$_4$N][BF$_4$]. Ferrocene was added as a calibrant after each set of measurements, and all potentials are quoted relative to that of the ferrocene-ferrocenium couple.

Synthesis of Platinum Polyyne Polymer **P1**

Polymerization was carried out by mixing **L$_1$** (50.0 mg, 0.143 mmol), *trans*-[PtCl$_2$(PBu$_3$)$_2$] (96.0 mg, 0.143 mmol) and CuI (5.0 mg) in Et$_3$N/CH$_2$Cl$_2$ (40 ml, 1:1, v/v). After stirring at room temperature overnight, the solution mixture was evaporated to dryness. The residue was redissolved in CH$_2$Cl$_2$ and filtered through a

short silica column using the same eluent to remove ionic impurities and catalyst residues. After removal of the solvent, the crude product was purified by precipitating it in CH_2Cl_2 from methanol several times. Subsequent washing with *n*-hexane and drying *in vacuo* gave a dark purple solid of **P1** (92.0 mg, 68%).

Solar Cell Fabrication and Characterization

ITO glass substrates (10 Ω □$^{-1}$) were cleaned by sonication in toluene, acetone, ethanol and deionized water, and dried in an oven. The samples were then cleaned with UV ozone for 300 s. As-received PEDOT:PSS solution was passed through the 0.45 μm filter and spin-coated on patterned ITO substrates at 5000 r.p.m. for 3 min. The substrates were then baked in N_2 at 150 ºC for 15 min. The **P1**:PCBM (1:4) active layer was prepared by spin-coating the toluene solution (4 mg ml^{-1} of **P1**, 16 mg ml^{-1} of PCBM) at 1000 r.p.m. for 2 min. The substrates were dried in a vacuum oven at room temperature for 1 h, and then stored in high vacuum (10^{-5}–10^{-6} Torr) overnight. Then, Al electrode (100 nm) was evaporated through a shadow mask to define the active area of the devices (2 mm and 4 mm diameter circles). For comparison purpose, solar cells with P3HT:PCBM (1:4) active layer were also prepared. The procedure for cell fabrication was the same as in the case of **P1**, except that P3HT:PCBM solution was prepared in chlorobenzene and stirred overnight in N_2 at 40 ºC. All the fabrication procedures were performed in air, while the cells were measured in N_2 inside the sealed sample holder with a quartz window. The current–voltage characteristics were measured using a Keithley 2400 sourcemeter. For white light efficiency measurements (at 100 mW cm^{-2}), Oriel 66002 solar light simulator with AM1.5 filter was used. The light intensity was measured by a Molectron Power Max 500D laser power meter. For the measurement of the external quantum efficiency, different wavelength of light was selected with a Thermo Oriel 257 monochromator. The photocurrent generated was measured with a Keithley 2400 sourcemeter. The light intensity was measured with a Newport 1830-C optical power meter equipped with a 818-UV detector probe. AFM images have been obtained using Seiko SPI 3800N Probe Station with SPA 300 HV Scanning Probe Microscope controller. The scanning speed was 0.1–0.3 Hz and the tip resonant frequency and force constant were 109 kHz and 16 N m^{-1}, respectively. The charge carrier mobility was determined by the time-of-flight method. The samples were prepared by drop-casting the blend on ITO glass. Toluene was used as a solvent for **P1**:PCBM (1:4) blend, while

chlorobenzene was used as a solvent for P3HT:PCBM (1:4) blend. The film thickness was 1.11 μm for **P1**:PCBM, and 2.45 μm for P3HT:PCBM. After drying the film in vacuum, Al electrode (50 nm) was evaporated in high vacuum (10^{-6} Torr). A nitrogen laser was used to generate pulsed excitation (λ = 337.1 nm). The transient photocurrent was monitored by an oscilloscope Tektronix TDS 3052 B. Due to different fabrication method, spin-coated films were also prepared and the mobilities were determined from the space-charge limited current modelling. For the hole mobility determination, device structure was ITO/PEDOT:PSS/blend film/Au, while for electron mobility determination the device configuration was ITO/Mg/blend film/LiF/Al. The mobilities were determined by fitting the measured I-V curves to SCLC model.[10] The relative permittivity of the material was estimated from the modified Lorentz model fitting[55] of the ellipsometry data. Spectroscopic ellipsometry measurements were performed using a JA Woollam V-VASE ellipsometer.

Received xxxxxx

References

1. Kim, J. Y. *et al.* New architecture for high-efficiency polymer photovoltaic cells using solution-based titanium oxide as an optical spacer. *Adv. Mater.* **18**, 572–576 (2006).
2. Reyes-Reyes, M., Kim, K. & Carroll, D. J. High-efficiency photovoltaic devices based on annealed poly(3-hexylthiophene) and 1-(3-methoxycarbonyl)-propyl-1-phenyl-(6,6)C_{61} blends. *Appl. Phys. Lett.* **87**, 083506-1–083506-3 (2005).
3. Kim, Y. *et al.* A strong regioregularity effect in self-organizing conjugated polymer films and high-efficiency polythiophene:fullerene solar cells. *Nature Mater*. **5**, 197–203 (2006).
4. Li, G. *et al*. High-efficiency solution processable polymer photovoltaic cells by self-organization of polymer blends. *Nature Mater.* **4**, 864–868 (2005).

5. Li, G., Shortriya, V., Yao, Y. & Yang, Y. Investigation of annealing effects and film thickness dependence of polymer solar cells based on poly(3-hexylthiophene). *J. Appl. Phys.* **98**, 043704-1–043704-5 (2005).
6. Kim, Y., Choulis, S. A., Nelson, J., Bradley, D. D. C., Cook, S. & Durrant, J. R. Device annealing effect in organic solar cells with blends of regioregular poly(3-hexylthiophene) and soluble fullerene. *Appl. Phys. Lett.* **86**, 063502-1–063502-3 (2006).
7. Chirvase, D., Parisi, J., Hummelen, J. C. & Dyakonov, V. Influence of nanomorphology on the photovoltaic action of polymer–fullerene composites**.** *Nanotechnology* **15**, 1317–1323 (2004).
8. De Bettignies, R., Leroy, J., Firon, M. & Sentein, C. Accelerated lifetime measurements of P3HT:PCBM solar cells. *Synth. Met.* **156**, 510–513 (2006).
9. Mihailetchi, V. D. *et al*. Origin of the enhanced performance in poly(3-hexylthiophene):[6,6]-phenyl C_{61} butyric acid methyl ester solar cells upon slow drying of the active layer. *Appl. Phys. Lett.* **89**, 012107-1–012107-3 (2006).
10. Mihailetchi, V. D., Xie, H., de Boer, B., Koster, L. J. A. & Blom, P. W. M. Charge transport and photocurrent generation in poly(3-hexylthiophene):methanofullerene bulk heterojunction solar cells. *Adv. Funct. Mater.* **16**, 699–708 (2006).
11. Koster, L. J. A., Mihailetchi, V. D. & Bloom, P. W. Ultimate efficiency of polymer/fullerene bulk heterojunction solar cells. *Appl. Phys. Lett.* **88**, 093511-1–093511-3 (2006).
12. Scharber, M. C. *et al*. Design rules for donors in bulk-heterojunction solar cells - Towards 10% energy-conversion efficiency. *Adv. Mater.* **18**, 789–794 (2006).
13. Wienk, M. M., Turbiez, M. G. R., Struijk, M. P., Fonrodona, M. & Janssen, R. Low-band gap poly(di-2-thienylthienopyrazine):fullerene solar cells. *Appl. Phys. Lett.* **88**, 153511–153513 (2006).
14. Wang, X. *et al*. Infrared photocurrent spectral response from plastic solar cell with low-band-gap polyfluorene and fullerene derivative. *Appl. Phys. Lett.* **85**, 5081–5083 (2004).

15. Wang, X., Perzon, E., Oswald, F., Langa, F., Andersson, M. R. & Inganäs, O. Enhanced photocurrent spectral response in low-bandgap polyfluorene and C_{70}-derivative-based solar cells. *Adv. Funct. Mater.* **15**, 1665–1670 (2005).

16. Xia, Y. *et al*. Novel random low-band-gap fluorene-based copolymers for deep red/near infrared light-emitting diodes and bulk heterojunction photovoltaic cells. *Macromol. Chem. Phys.* **207**, 511–520 (2006).

17. Zhou, Q., Hou, Q., Zheng, L., Deng, X., Yu, G. & Cao, Y. Fluorene-based low band-gap copolymers for high performance photovoltaic devices. *Appl. Phys. Lett.* **84**, 1653–1655 (2004).

18. Svensson, M. *et al.* High-performance polymer solar cells of an alternating polyfluorene copolymer and a fullerene derivative. *Adv. Mater.* **15**, 988–991 (2003).

19. Shi, C., Yao, Y., Yang, Y. & Pei, Q. Regioregular copolymers of 3-alkoxythiophene and their photovoltaic application. *J. Am. Chem. Soc.* **128**, 8980–8986 (2006).

20. Zhang, F., Mammo, W., Andersson, L. M., Admassie, S., Andersson, M. R., & Inganäs, O. Low-bandgap alternating fluorene copolymer/methanofullerene heterojunctions in efficient near-infrared polymer solar cells. *Adv. Mater.* **18**, 2169–2173 (2006).

21. Hou, J., Tan, Z., Yan, Y., He, Y., Yang, C., & Li, Y. Synthesis and photovoltaic properties of two-dimensional conjugated polythiophenes with bi(thienylenevinylene) side chains. *J. Am. Chem. Soc.* **128**, 4911–4916 (2006).

22. Mühlbacher, D. *et al*. High photovoltaic performance of a low-bandgap polymer, *Adv. Mater*. **18**, 2884–2889 (2006).

23. Zhang, F., Perzon, E., Wang, X., Mammo, W., Andersson, M. R., & Inganäs, O. Polymer solar cells based on a low-bandgap fluorene copolymer and a fullerene derivative with photocurrent extended to 850 nm. *Adv. Funct. Mater.* **18**, 2169–2173 (2006).

24. Brabec, C. J. *et al*. A low-bandgap semiconducting polymer for photovoltaic devices and infrared emitting diodes. *Adv. Funct. Mater.* **12**, 709–712 (2002).

25. Shaheen, S. A. *et al*. Low band-gap polymeric photovoltaic devices. *Synth. Met.* **121**, 1583–1584 (2001).

26. Xue, J., Uchida, S., Rand, B. P. & Forrest, S. R. 4.2% Efficient organic photovoltaic cells with low series resistances. *Appl. Phys. Lett.* **84**, 3013–3015 (2004).

27. Robertson, N. Optimizing dyes for dye-sensitized solar cells. *Angew. Chem. Int. Ed.* **45**, 2338–2345 (2006).

28. Chawdhury, N. *et al.* Evolution of lowest singlet and triplet excited states with number of thienyl rings in platinum poly-ynes. *J. Chem. Phys.* **110**, 4963–4970 (1999).

29. Köhler, A., Wittman, H. F., Friend, R. H., Khan, M. S., Lewis, J. Enhanced photocurrent response in photocells made with platinum-poly-yne/C_{60} blends by photoinduced electron transfer. *Synth. Met.* **77**, 147–150 (1996).

30. Guo, F., Kim, Y.-G., Reynolds, J. R., & Schanze, K. S. Platinum-acetylide polymer based solar cells: involvement of the triplet state for energy conversion. *Chem. Commun.* **2006**, 1887–1889 (2006).

31. Younus, M. *et al.* Synthesis, electrochemistry, and spectroscopy of blue platinum(II) polyynes and diynes. *Angew. Chem. Int. Ed.* **37**, 3036–3039 (1998).

32. Wilson, J. S., Dhoot, A. S., Seeley, A. J. A. B., Khan, M. S., Köhler, A. & Friend, R. H. Spin-dependent exciton formation in π-conjugated compounds. *Nature* **413**, 828–831 (2001).

33. Manners, I. Putting metals into polymers. *Science* **294**, 1664–1666 (2001).

34. Long, N. J. & Williams, C. K. Metal alkynyl σ complexes: Synthesis and materials. *Angew. Chem. Int. Ed.* **42**, 2586–2617 (2003).

35. Manners, I. *Synthetic metal-containing polymers*. Wiley-VCH, Weinheim (2004).

36. Köhler, A. & Beljonne, D. The singlet-triplet exchange energy in conjugated polymers. *Adv. Funct. Mater.* **14**, 11–18 (2004).

37. Wong, W.-Y. Recent advances in luminescent transition metal polyyne polymers. *J. Inorg. Organomet. Polym. Mater.* **15**, 197–219 (2005).

38. Karikomi, M., Kitamura, C., Tanaka, S. & Yamashita, Y. New narrow-bandgap polymer composed of benzobis(1,2,5-thiadiazole) and thiophenes. *J. Am. Chem. Soc.* **117**, 6791–6792 (1995).

39. Roncali, J. Synthetic principle for bandgap control in linear π-conjugated systems. *Chem. Rev.* **97**, 173–205 (1997).

40. Wong, W.-Y., Choi, K.-H., Lu, G.-L. & Shi, J.-X. Synthesis, redox and optical properties of low-bandgap platinum(II) polyynes with 9-dicyanomethylene-substituted fluorene acceptors. *Macromol. Rapid Commun.* **22**, 461–465 (2001).

41. Bredas, J. L. Theoretical design of polymeric conductors. *Synth. Met.* **17**, 115–121 (1987).

42. Köhler, A. *et al.* Donor-acceptor interactions in organometallic and organic poly-ynes. *Synth. Met.* **101**, 246–247 (1999).

43. Bredas, J. L., Heeger, A. J. & Wudi, F. Towards organic polymers with very small intrinsic band gaps. I. Electronic structure of polyisothianaphthene and derivatives. *J. Chem. Phys.* **85**, 4673–4678 (1986).

44. Havinga, E. E., Haeve, W. & Wynberg, H. Alternate donor-acceptor small-band-gap semiconducting polymers: Polysquaraines and polycroconaines. *Synth. Met.* **55–57**, 299–306 (1993).

45. Kertesz, M & Lee, Y.-S. Electronic structures of small gap polymers. *Synth. Met.* **28**, C545–552 (1989).

46. Wong, W.-Y. & Ho, C.-L. Di-, oligo- and polymetallaynes: Synthesis, photophysics, structures and applications. *Coord. Chem. Rev.* **250**, 2627–2690 (2006).

47. Wilson, J. S. *et al.* The energy gap law for triplet states in Pt-containing conjugated polymers and monomers. *J. Am. Chem. Soc.* **123**, 9412–9417 (2001).

48. Ashraf, R. S., Shahid, M., Klemm, E., Al-Ibrahim, M. & Sensfuss, S. Thienopyrazine-based low-bandgap poly(heteroaryleneethynylene)s for photovoltaic devices. *Macromol. Rapid Commun.* **27**, 1454–1459 (2006).

49. van Duren, J. K. J. *et al.* Relating the morphology of poly(*p*-phenylene vinylene)/methanofullerene blends to solar-cell performance. *Adv. Funct. Mater.* **14**, 425–434 (2004).

50. Mihailetchi, V. D. *et al*. Compositional dependence of the performance of poly(*p*-phenylene vinylene):methanofullerene bulk-heterojunction solar cells. *Adv. Funct. Mater.* **15**, 795–801 (2005).

51. Shikler, R., Chiesa, M. & Friend, R. H. Photovoltaic performance and morphology of polyfluorene blends: The influence of phase separation evolution. *Macromolecules* **39**, 5393–5399 (2006).

52. Huang, J., Li, G. & Yang, Y. Influence of composition and heat-treatment on the charge transport properties of poly(3-hexylthiophene) and (6,6)-phenyl C_{61}–butyric acid methyl ester blends. *Appl. Phys. Lett.* **87**, 112105-1–112105-3 (2005).

53. von Hauff, E., Parisi, J., & Dyakonov, V. Investigations of the effects of tempering and composition dependence on charge carrier field effect mobilities in polymer and fullerene films and blends. *J. Appl. Phys.* **100**, 043702-1–043702-7 (2006).

54. Shrotriya, V., Li, G., Yao, Y., Moriarty, T., Emery, K. & Yang, Y. Accurate measurement and characterization of organic solar cells. *Adv. Funct. Mater.* **16**, 2016–2023 (2006).

55. Liu, Z. T., Kwok, H. S., Djurišić, A. B. The optical functions of metal phthalocyanines. *J. Phys. D: Appl. Phys.* **37**, 678–688 (2004).

Acknowledgements

This work was supported by the Research Grants Council of The Hong Kong Special Administrative Region, China (Project Numbers HKBU 2024/04P, HKU 7008/04P, and 7010/05P). Financial support from the Hong Kong Baptist University, and Strategic Research Theme, University Development Fund, and Seed

Funding Grant and Outstanding Young Researcher Award (administrated by The University of Hong Kong) are also acknowledged. The authors would like to thank Dr. J. Gao from the University of Hong Kong for step-profiler thickness measurements, A. M. C. Ng for ellipsometry measurements, and Dr. W. C. H. Choy and HKU-CAS Joint Laboratory on New Materials and Prof. C. M. Che for the use of glove box for encapsulation. The authors would also like to thank Dr. R. de Bettignies and Dr. S. Guillerez from CEA-INES RDI, Laboratoire Composants Solaires, in Bourges Du Lac, France for independent verification of the solar cell results.

Correspondence and requests should be addressed to W.-Y.W. or A.B.D.

Supplementary Information accompanies this paper on www.nature.com/naturematerials.

Competing financial interests

The authors declare that they have no competing financial interests.

Legends for Scheme and Figures

Scheme 1 Synthesis of low band gap organometallic diyne and polyyne.

Figure 1 Solid-state structure of **M1**. A perspective view of the crystal structure of the model complex **M1**.

Figure 2 Optical properties of $\mathbf{L_1}$, **P1**, and **M1.** a) Absorption spectra of $\mathbf{L_1}$, **P1**, and **M1** b) Emission spectra of $\mathbf{L_1}$, **P1**, and **M1** in solution c) Emission spectra of **P1** films at different temperatures.

Figure 3 *J–V* curves of solar cells with **P1**:PCBM (1:4) (solid line) and P3HT:PCBM (1:4) (dashed line) active layers. a) *J–V* curves in the dark b) *J–V* curves under simulated AM1.5 solar irradiation.

Figure 4 AFM images of **P1**:PCBM films for different blend compositions. Topography (left) and phase contrast (right) images of bulk heterojunction films a,b) **P1**:PCBM 1:4; c,d) **P1**:PCBM 1:1. The area is 2 μm × 2 μm.

Figure 5 Comparison of **P1**:PCBM and P3HT:PCBM blends. a) EQE wavelength dependencies of solar cells with **P1**:PCBM (1:4) (closed circles) and P3HT:PCBM (1:4) (open circles) active layers. The absorption of the **P1**:PCBM active layer is shown in the inset. Electrical field dependence of b) electron and c) hole mobility of **P1**:PCBM (1:4) (closed circles) and P3HT:PCBM (1:4) (open circles) blends. Real d) and imaginary e) parts of the refractive index of **P1:**PCBM and P3HT:PCBM films determined by spectroscopic ellipsometry.

Figure 6 Performance of **P1**:PCBM device for different illumination powers. a) *J–V* curves. Power dependences of b) open circuit voltage (open triangles), fill factor (closed triangles); c) short circuit current density (closed circles), power conversion efficiency (open circles).

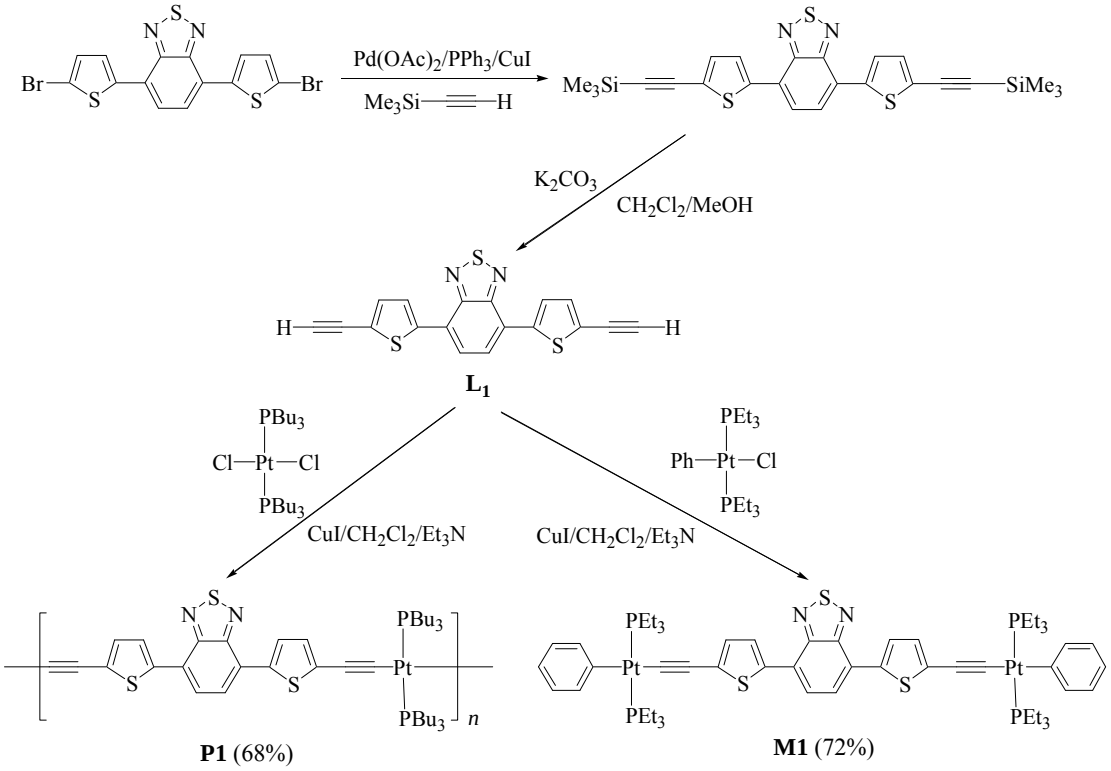
Br
Br
Pd(OAc)2/PPh3/CuI
Me3Si—≡—H
Me3Si
SiMe3
K2CO3
CH2Cl2/MeOH
H
H
L1
PBu3
Cl—Pt—Cl
PBu3
CuI/CH2Cl2/Et3N
PEt3
Ph—Pt—Cl
PEt3
CuI/CH2Cl2/Et3N
PBu3
PBu3
n
PEt3
PEt3
PEt3
PEt3
P1 (68%)
M1 (72%)

Scheme 1

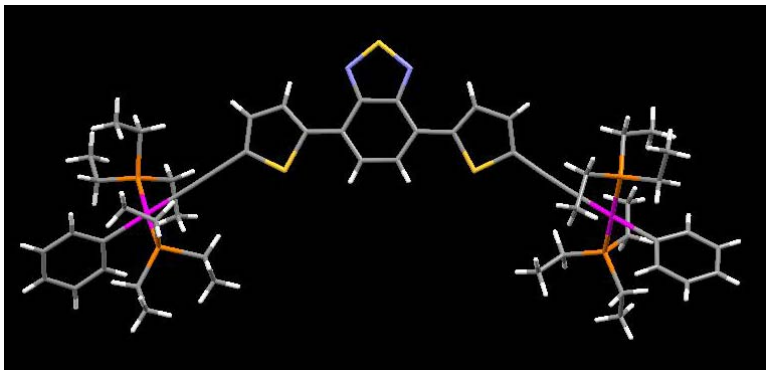

Figure 1

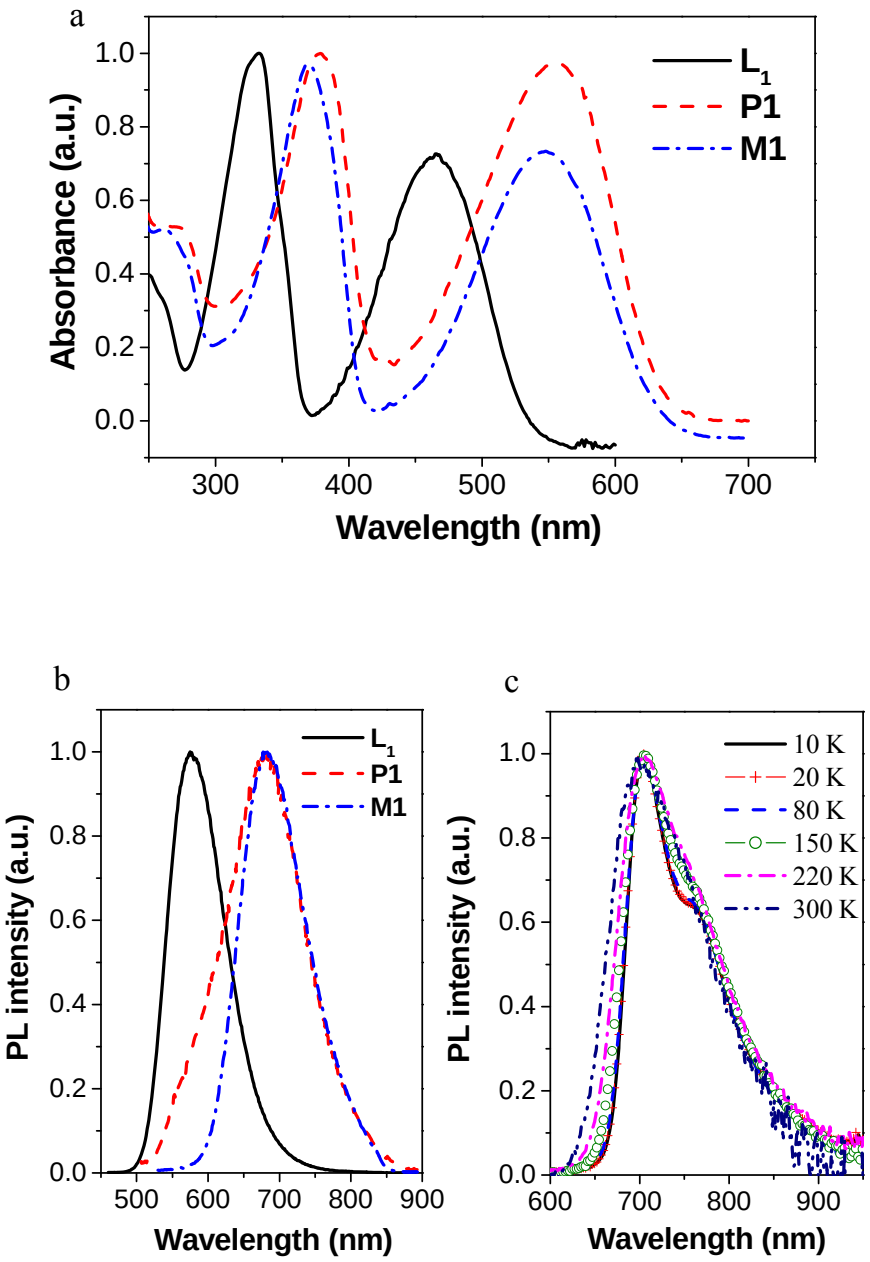
a
Absorbance (a.u.)
Wavelength (nm)
L1
P1
M1
b
PL intensity (a.u.)
Wavelength (nm)
L1
P1
M1
c
PL intensity (a.u.)
Wavelength (nm)
10 K
20 K
80 K
150 K
220 K
300 K

Figure 2.

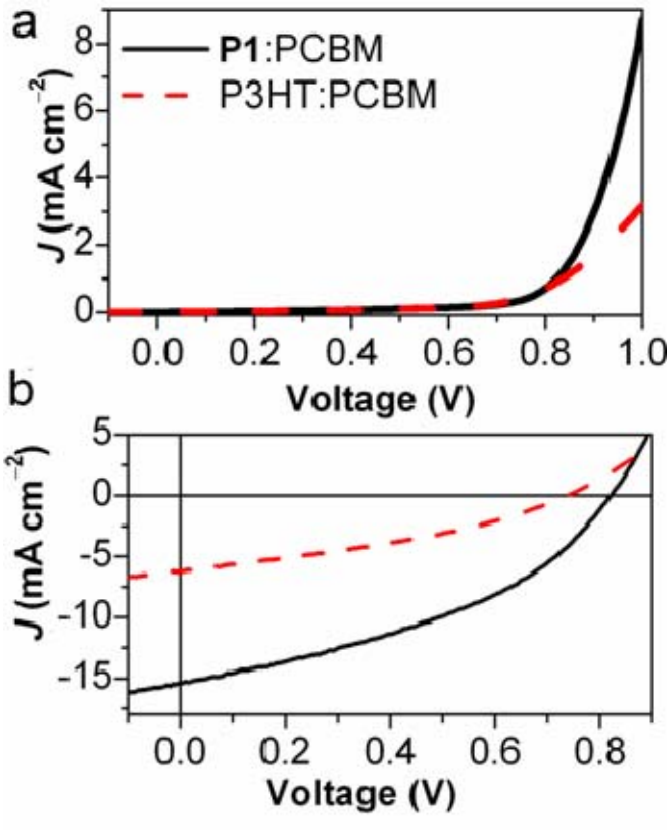

Figure 3

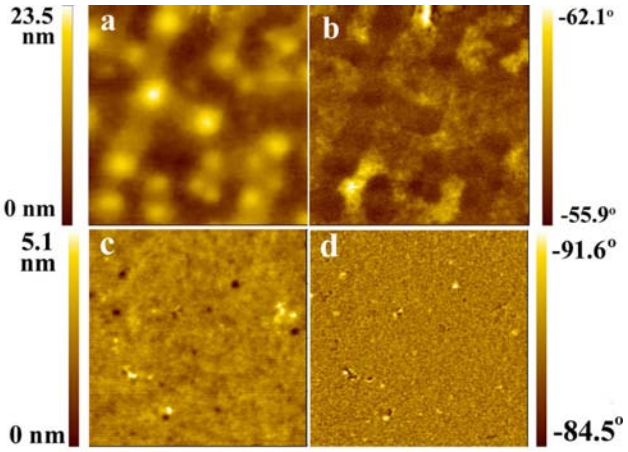

Figure 4

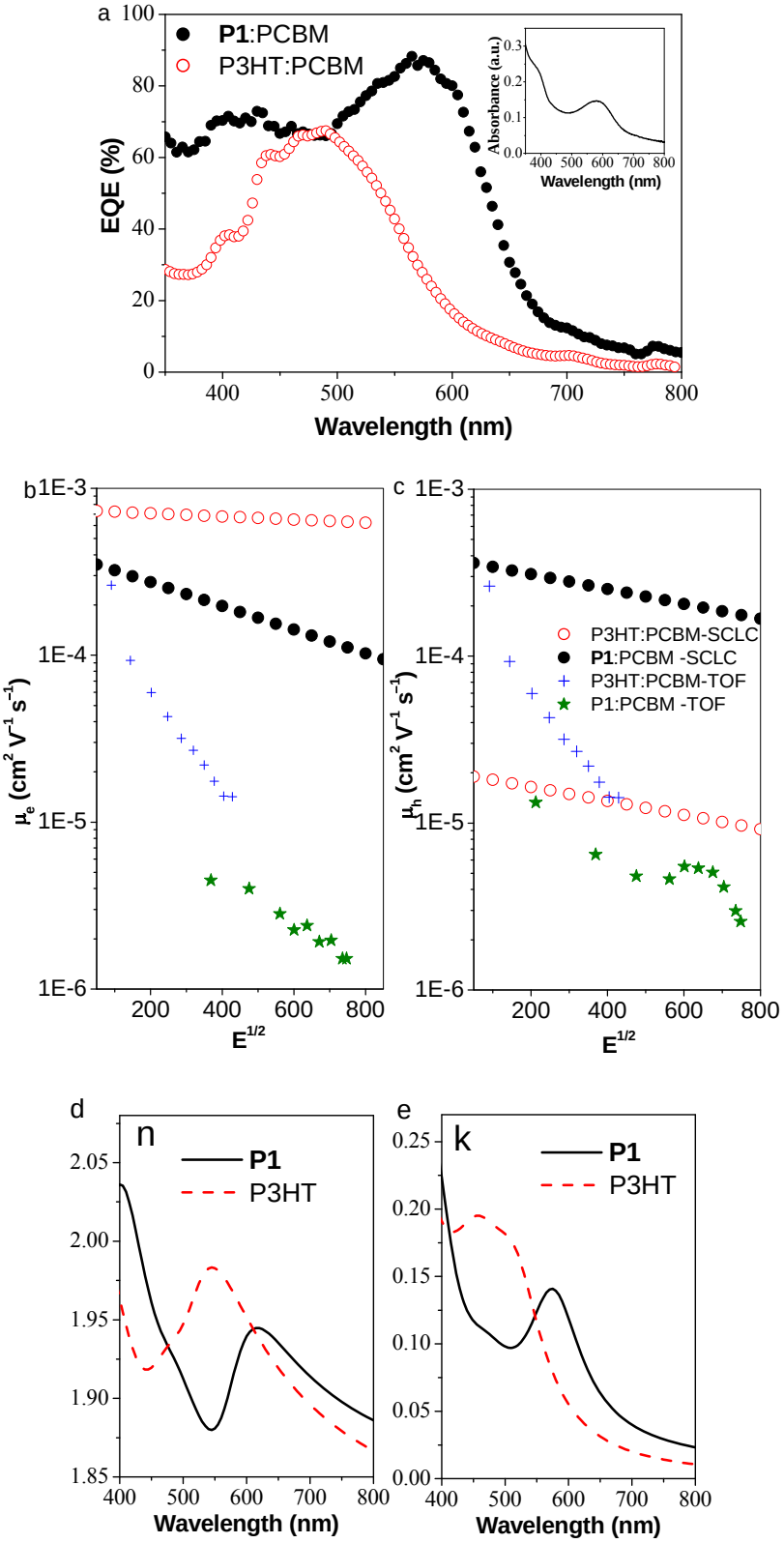
a
P1:PCBM
P3HT:PCBM
EQE (%)
Wavelength (nm)
Absorbance (a.u.)
Wavelength (nm)
b
c
P3HT:PCBM-SCLC
P1:PCBM -SCLC
P3HT:PCBM-TOF
P1:PCBM -TOF
E1/2
d
n
P1
P3HT
Wavelength (nm)
e
k
P1
P3HT
Wavelength (nm)

Figure 5

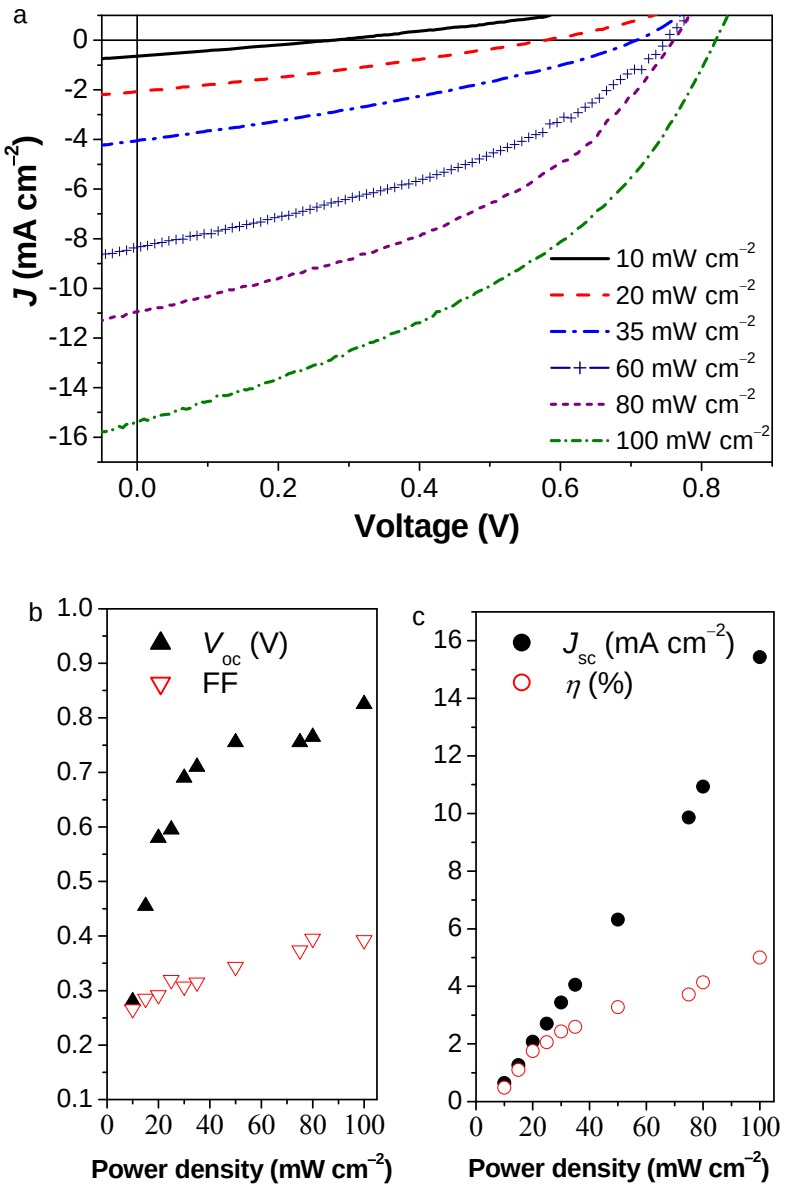
a
J (mA cm^{-2})
Voltage (V)
10 mW cm^{-2}
20 mW cm^{-2}
35 mW cm^{-2}
60 mW cm^{-2}
80 mW cm^{-2}
100 mW cm^{-2}
b
V_{oc} (V)
FF
Power density (mW cm^{-2})
c
J_{sc} (mA cm^{-2})
η (%)
Power density (mW cm^{-2})

Figure 6

Suggestion for the Table of Contents